Radiation Properties of Moving Constellations of (nano) Satellites: A Complexity Study

Wessel P. Bruinsma[1], Robin P. Hes[1], Sjoerd Bosma[1], Ioan E. Lager[1], and Mark J. Bentum[2]

[1]Delft University of Technology, Faculty of Electrical Engineering, Mathematics and Computer Science,
Mekelweg 4, 2628 CD Delft, the Netherlands,

[2]University of Twente, Faculty of Electrical Engineering, Mathematics and Computer Science,
7500 AE Enschede, the Netherlands,

Emails: i.e.lager@tudelft.nl,m.j.bentum@utwente.nl

Abstract—The (computational) complexity involved by beamforming in moving constellations of (nano) satellites is investigated by means of illustrative numerical experiments. While the number of radiators in such three-dimensional (3D) array antennas is not large, evaluating their radiation patterns entails challenging computational intricacies in view of the satellites being in motion and each satellite performing general 3D rotations. As a result, the relevant array radiation patterns become time-dependent, the elementary radiation patterns being themselves time-dependent. The discussed experiments will illustrate the time evolution of the radiation pattern for given individual satellite orbits and rotation laws. At the same time, they will provide a basis for estimating the computational complexity involved by predicting the complete beamforming in future space-bound remote sensing missions using constellations of (nano) satellites.

I. INTRODUCTION

In the past few decades, radio astronomy was the main driving force in the quest towards understanding the origin and the evolution of the Universe. Presently, Earth based and space platforms effectively cover the vast majority of the electromagnetic (EM) spectrum. Recently, space-bound instrumentation has concentrated on the (low) Terahertz spectrum, with the Herschel Space Observatory offering groundbraking discoveries on the Universe's structure and evolution and the SPace Infrared telescope for Cosmology and Astrophysics (SPICA) [1] mission being expected to drastically widen the exploration capabilities in that range.

Nonetheless, the 0.3–30 MHz frequency range is, practically, unexplored. This situation may seem surprising, since this spectrum allows studying the early Cosmos at high hydrogen red shifts, the so-called dark ages, extragalactic surveys, (extra) solar planetary bursts and high energy particle physics [2]. The reason for the lack of measurements in the 0.3–30 MHz range is twofold: On the one hand, Earth-bound reception in this range is severely hampered [2]–[4] due to the ionosphere and by Earth bounded radio-frequency interference. On the other hand, space-bound observation requires huge apertures, that are not practical with present-day technology.

A particularly promising solution to performing studies in this range is by using constellations of remote sensing (nano) satellites. This strategy is at the centre of the proposed Orbiting Low Frequency Antennas for Radio Astronomy (OLFAR) distributed radio telescope [3]–[5]. The practical realisation of OLFAR builds up on recent progress in Earth-bound, large aperture, distributed radio astronomy. However, straightforwardly porting the relevant technologies to satellite constellations is impossible due to the inherent computing and communication limitations of space-bound platforms. Consequently, effective measures are now sought for ensuring the tractability of the implementation of OLFAR.
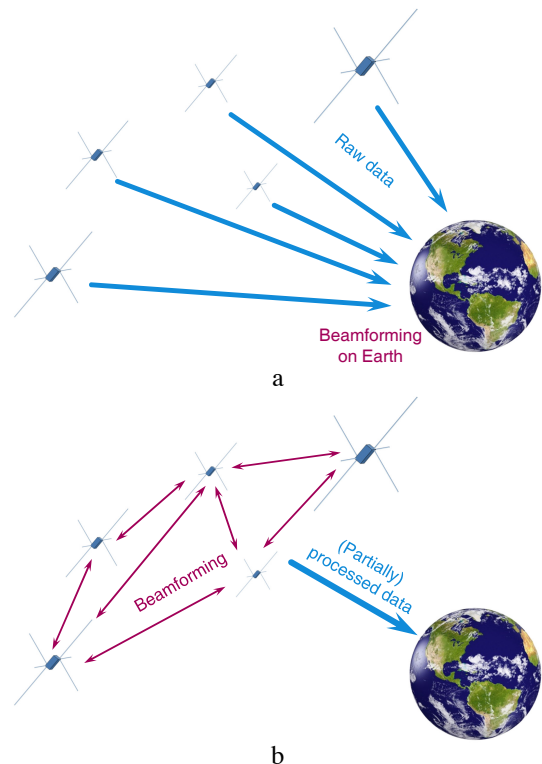

Fig. 1. Processing variants for the OLFAR concept. (a) Raw data transmission and beamforming on Earth; (b) beamforming in the constellation and transmission of (partially) processed data.

In this respect, it is noted that the sensing satellite clusters can be construed as sparse, random, three-dimensional (3D) array antennas [6]. As with any array antenna, pointing the beam to radio sources of choice requires beamforming the received signals. Here, two avenues are available: transferring the full raw digital data to Earth and performing the beamforming there (see Fig. 1.a) or beamforming at the constellation level and transferring only (partially) processed information to Earth (see Fig. 1.b). Although relying on the huge computing resources that are readily available on Earth, the former avenue can be

easily ruled out on grounds of the achievable communication channel capacities being largely insufficient for transferring the immense quantity of raw data even when state-of-the-art compression techniques were applied to this end. This observation applies the more so when the constellations are at (relatively) large distances from the Earth. On the contrary, the latter strategy may result in a significantly smaller amount of data that may, in principle, be accommodated within the channel capacity. However, the computational resources within the constellation are limited, this demanding a careful tailoring of the processing algorithms.

This papers investigates the (computational) complexity involved by the 3D array beamforming. The task's intricacy is largely enhanced by the fact that, in view of limited fuel availability, the spatial orientation of the satellites cannot be but seldom corrected. Consequently, apart from moving along prescribed orbits, the satellites also perform general 3D rotations. Consequently, beamforming will be necessarily carried out based on the satellites' *time-dependent, non-identical* elementary radiation patterns.

The paper starts by describing the investigated configuration. A framework is then given for evaluating the radiation patterns of 3D array antennas with moving elements. The radiation from rotating satellites and some important aspects concerning moving EM radiators are elaborated upon in the Appendix. The theoretical ideas will be illustrated via numerical experiments and, finally, conclusions will be drawn.

II. EXAMINED CONFIGURATION

The present study concerns a general 3D configuration. In it, position is specified by the coordinates $\{x, y, z\}$ with respect to a background Cartesian reference frame with origin $\mathcal{O}$ and three mutually orthogonal unit vectors $\{\hat{\boldsymbol{x}}, \hat{\boldsymbol{y}}, \hat{\boldsymbol{z}}\}$ that, in this order, form a right-handed system. The position vector is $\boldsymbol{r} = x\hat{\boldsymbol{x}} + y\hat{\boldsymbol{y}} + z\hat{\boldsymbol{z}}$, with $|\boldsymbol{r}| = r$ and $\hat{\boldsymbol{\xi}} = \boldsymbol{r}/r$. A ('universal') spherical coordinate system with the same origin and coordinates $\{\vartheta, \varphi\}$ is also considered, ϑ measuring the tilting from $\hat{\boldsymbol{z}}$ and φ the trigonometric rotation from $\hat{\boldsymbol{x}}$. Correspondingly, the three mutually orthogonal unit vectors $\{\hat{\boldsymbol{\vartheta}}, \hat{\boldsymbol{\varphi}}, \hat{\boldsymbol{\xi}}\}$ form, in this order, a right-handed system. This coordinate system will be employed as a basis for evaluating the radiation patterns of the investigated antenna system. Note that $\hat{\boldsymbol{\xi}}$ and $\{\vartheta, \varphi\}$ will be hereafter used interchangeably for defining an observation direction. The time coordinate is t.

The configuration consists of N *identical* (nano) satellites. The antenna system of each satellite consists of 3 reciprocally orthogonal dipole antennas, their lengths being l_k ($k = 1, 2, 3$). The reference centre of each satellite, that is also taken as the reference centre of the relevant antenna system, is $\boldsymbol{r}'_n(t)$ ($n = 1, \ldots, N$), the trajectories $\boldsymbol{r}'_n(t)$ being assumed known. Each satellite is allowed to perform general 3D rotations, the corresponding, *time-dependent* Euler angles [7, Section 4.4][†] $\alpha_n(t)$, $\beta_n(t)$ and $\gamma_n(t)$ being also assumed known.

The excitation of the antenna systems is taken to be time-harmonic, with frequency f and angular frequency $\omega = 2\pi f$.

[†]Denoting the Euler angles as α, β and γ is preferred in this paper for avoiding confusions with the $\{\vartheta, \varphi\}$ coordinates in the 'universal' spherical reference frame. The following correspondence with the notation in [7, Section 4.4] holds: $\alpha \leftrightarrow \phi$, $\beta \leftrightarrow \theta$ and $\gamma \leftrightarrow \psi$.

The satellites radiate in free space, with electric permittivity ϵ_0, magnetic permeability μ_0 and wavespeed $c_0 = (\epsilon_0\mu_0)^{-\frac{1}{2}}$. Correspondingly, the wavenumber is $k_0 = \omega/c_0$ and the wavelength is $\lambda = c_0/f$. Furthermore, the vectorial wavenumber is $\boldsymbol{k} = \boldsymbol{k}(\vartheta, \varphi) = k_x\boldsymbol{i}_x + k_y\boldsymbol{i}_y + k_z\boldsymbol{i}_z$, with

$$k_x = k_0 \sin(\vartheta) \cos(\varphi) \tag{1}$$
$$k_y = k_0 \sin(\vartheta) \sin(\varphi) \tag{2}$$
$$k_z = k_0 \cos(\vartheta) \tag{3}$$

for $\vartheta \in [0, \pi]$ and $\varphi \in [0, 2\pi)$.

III. RADIATION PROPERTIES OF CONSTELLATION OF SATELLITES IN MOTION

In line with [6], [8], the far-field (electric field strength) characteristic[‡] radiated by an array in the observation direction $\boldsymbol{\xi}$ is expressed as

$$\boldsymbol{E}^\infty(\hat{\boldsymbol{\xi}}) = \sum_{n=1}^{N} \left\{ \boldsymbol{E}_n^\infty(\hat{\boldsymbol{\xi}}) \exp\left[-\mathrm{j}\left(\boldsymbol{k} - \boldsymbol{k}_{\mathrm{sc}}\right)\cdot\boldsymbol{r}'_n\right] \right\} \tag{4}$$

in which $\boldsymbol{E}_n^\infty(\hat{\boldsymbol{\xi}})$ ($n = 1, \ldots, N$) are the far-field characteristics of the satellites, $\boldsymbol{r}'_n = \boldsymbol{r}_n - \boldsymbol{r}_{\mathrm{c}}$, with $\boldsymbol{r}_n$ being the position vectors of the individual radiators and $\boldsymbol{r}_{\mathrm{c}}$ the position vector of the array antenna's reference centre and the terms $\exp\left(\mathrm{j}\boldsymbol{k}_{\mathrm{sc}}\cdot\boldsymbol{r}'_n\right)$ represent the progressive phase shift, with $\boldsymbol{k}_{\mathrm{sc}} = \boldsymbol{k}(\boldsymbol{\xi}_{\mathrm{sc}})$ corresponding to the scanning direction $\boldsymbol{\xi}_{\mathrm{sc}}$ (given by $\{\vartheta_{\mathrm{sc}}, \varphi_{\mathrm{sc}}\}$).

However, unlike in the cases studied in [6], [8], the constellations of satellites investigated in this paper *are in motion*. Consequently, (4) must be adjusted as

$$\boldsymbol{E}^\infty(\hat{\boldsymbol{\xi}}, t) = \sum_{n=1}^{N} \left\{ \boldsymbol{E}_n^\infty(\hat{\boldsymbol{\xi}}, t) \exp\left[-\mathrm{j}\left(\boldsymbol{k} - \boldsymbol{k}_{\mathrm{sc}}\right)\cdot\boldsymbol{r}'_n(t)\right] \right\} \tag{5}$$

in which $\boldsymbol{E}_n^\infty(\hat{\boldsymbol{\xi}}, t)$ account for the *known rotation* of the satellites (see the derivation in Appendix A) while $\boldsymbol{r}'_n(t) = \boldsymbol{r}_n(t) - \boldsymbol{r}_{\mathrm{c}}(t)$ account for their *known trajectories*.

Note that in formulating (5) use was made of the "low-velocity approximation" (see Appendix B for details). In view of this assumption, the individual satellites' radiation can be decoupled from their motion. Here, it can be reasonably expected that the low-velocity approximation is applicable to the *relative velocities* $\partial_t\boldsymbol{r}'_n(t)$ and to the angular velocities of the satellite rotations. However, its applicability to the *absolute velocity* $\partial_t\boldsymbol{r}_{\mathrm{c}}(t)$ deserves a detailed analysis and will have to be assessed on a case-to-case basis. In view of the feasibility character of this study, the low-velocity approximation will be hereafter consistently accounted for.

As stressed in [8], (4) and (5) do not allow the usual factoring of the radiated field into an element and an array characteristics. The polarisation pattern of the radiated field is extremely intricate and, moreover, time-dependent in (5). This may be a matter of concern when polarisation matching with a target may be needed. Addressing this aspect is outside the scope of this analysis.

[‡]The far-field characteristic [10, Eq. (9)] follows from the corresponding far-field quantities, by ignoring the $(4\pi r)^{-1}$ dependence.

The satellite constellations are only expected to sense radiated power. Consequently, evaluating the radiation pattern of the relevant 3D array antennas will suffice. As usually, the directivity pattern [9, Section 2.2], [10] is expressed as

$$D(\hat{\boldsymbol{\xi}}, t) = \frac{4\pi \left[\boldsymbol{E}^\infty(\hat{\boldsymbol{\xi}}, t) \cdot \boldsymbol{E}^{\infty *}(\hat{\boldsymbol{\xi}}, t) \right]}{\int\limits_{\hat{\boldsymbol{\xi}}' \cdot \hat{\boldsymbol{\xi}}' = 1} \left[\boldsymbol{E}^\infty(\hat{\boldsymbol{\xi}}', t) \cdot \boldsymbol{E}^{\infty *}(\hat{\boldsymbol{\xi}}', t) \right] d\Omega} \quad (6)$$

with '*' denoting complex conjugation and the integration being extended over all observation directions. Evidently, the directivity pattern will be time-dependent.

IV. ILLUSTRATIVE NUMERICAL EXPERIMENTS

The framework discussed in the section above is now applied to a constellation of 5 satellites. In line with [14], the satellite antenna systems operate at $40\,\mathrm{MHz}$. Two of the antennas are $9.6\,\mathrm{m}$ long, with the third being $0.3\,\mathrm{m}$ longer. The satellites are located in a *fixed* planar, rectangular cross layout, the distance between the satellites' reference centres being λ_0 at $40\,\mathrm{MHz}$. The satellites are taken to be initially aligned and are allowed to rotate, the Euler angular frequencies $\omega_{\alpha,n} = \partial_t \alpha_n$, $\omega_{\beta,n} = \partial_t \beta_n$, and $\omega_{\gamma,n} = \partial_t \gamma_n$, $n = 1, \ldots, 5$, having the *constant* values $0\,\mathrm{rad/s}$, $1\,\mathrm{rad/s}$ and $2\,\mathrm{rad/s}$, respectively. The Euler angular frequencies are deliberately taken different such that to better illustrate the time evolution of the radiation patterns as a result of the relative rotations.

In all examined cases, the array is scanned at $\{\vartheta_{\mathrm{sc}}, \varphi_{\mathrm{sc}}\} = \{0°, 0°\}$. In view of symmetry, the *array factor* exhibits a secondary (image) lobe at $\{180°, 0°\}$. Moreover, the chosen inter-element spacing leads to the onset of *array factor* grating lobes at $\{90°, 0°\}$, $\{90°, 90°\}$, $\{90°, 180°\}$ and $\{90°, 270°\}$, respectively. The rotation of the dipoles will affect the main, secondary and grating lobes' amplitude and, in some cases, may also result in a minor squinting of these lobes.

A. Rotation dependent radiation patterns

A first set of numerical experiments concerns the sampling of the radiation patterns at successive instants $t = 0$, 0.2, 0.4 and 0.6 seconds. The relevant snapshots are shown in Fig. 2. The transformations that the radiation patterns undergo as a result of the satellite rotations are clearly visible. The radiation pattern evolves from the original, desired version in Fig. 2.a to the situations in Fig. 2.c,d having no clear main beam and, thus, of no practical value.

B. Integrated array processing

Beamforming requires transferring the (digitised) received information from each nano-satellite to a central hub where it is processed. This results in a huge amount of data having to be transferred that, in turn, places very high demands on the relevant transmission channel. One effective way for drastically reducing the amount of transferred data is by integrating the received electric field at each satellite and relaying only the integrated data to the central hub.

The effect of integration is illustrated in Fig. 3. For consistency with the previous analysis, the integration is extended until the same instants $t = 0$ (no integration), 0.2, 0.4 and 0.6

seconds. The employed algorithm is based on a fine sampling of the integration interval (the time step being $\Delta_t = 0.01\,\mathrm{s}$) and a numerical integration via the rectangular rule. From the plots it can be inferred that resorting to integration not only that reduces the amount of transferred data but also tempers the (rate of) deterioration of the radiation pattern.

C. Discussion

The pattern evolutions examined in Sections IV-A and IV-B illustrate a rapid and accentuated deterioration of the cluster's radiation pattern. It must be stressed that, for highlighting the effect of the satellites' rotation on beamforming, the angular velocities were chosen disproportionately large. In a practical case, the integration time would be chosen such that, for the estimated angular velocities of the satellites, the total rotation between re-gauging and re-beamforming to be limited. Nevertheless, the present analysis provides insight in the effect of the individual rotations and, thus, offers a handle to finding an optimal balance between an acceptable pattern deterioration and integration time (and, implicitly, data traffic).

V. CONCLUSIONS

The effect of general 3D rotations of the (nano) satellites on the radiation pattern of constellations was examined by means of illustrative numerical experiments. The time-dependent character of the elementary radiation patterns to be beamformed directly influences the (computational) complexity involved by beamforming. The effect of individual pattern integration over suitably chosen periods was also evidenced. The analysis provides insight in the expected effect of satellites' the 3D rotations on the total radiation pattern. In this manner, it offers a handle to finding an optimal balance between pattern deterioration and integration time.

APPENDIX

A. Radiation properties of rotating satellites

As stated in Section II, all N (nano) satellites are identical, their antenna systems consisting of 3 reciprocally orthogonal dipoles of lengths l_k ($k = 1, 2, 3$). Without loss of generality, the dipoles are taken to be oriented along $\hat{\boldsymbol{d}}_{n,1} = \hat{\boldsymbol{x}}$, $\hat{\boldsymbol{d}}_{n,2} = \hat{\boldsymbol{y}}$ and $\hat{\boldsymbol{d}}_{n,3} = \hat{\boldsymbol{z}}$ ($n = 1, \ldots, N$), respectively. Each satellite performs general 3D rotations, the corresponding, time-dependent Euler angles $\alpha_n(t)$, $\beta_n(t)$ and $\gamma_n(t)$ being known. The radiation from individual satellites is henceforth discussed.

Based on [9, Eq. (4.62.a)], the far-field (electric field strength) characteristic corresponding to a dipole of length l and oriented along $\hat{\boldsymbol{z}}$ has the expression

$$E_\vartheta^\infty(I, l, \hat{\boldsymbol{\xi}}) = \mathrm{j}\eta_0 2I \exp(-\mathrm{j}k_0 r) \frac{\cos[\theta_l \cos(\vartheta)] - \cos(\theta_l)}{\sin(\vartheta)}$$

$$(7)$$

where I is the feeding current and

$$\theta_l = k_0 l / 2 = \pi l / \lambda_0. \quad (8)$$

Applying L'Hospital's rule in (7) entails that $\lim\limits_{\vartheta \downarrow 0} E_\vartheta^\infty(\hat{\boldsymbol{\xi}}) = \lim\limits_{\vartheta \uparrow \pi} E_\vartheta^\infty(\hat{\boldsymbol{\xi}}) = 0$, with $\vartheta \downarrow 0$ implying $\hat{\boldsymbol{\xi}} \to \hat{\boldsymbol{z}}$ and $\vartheta \uparrow \pi$
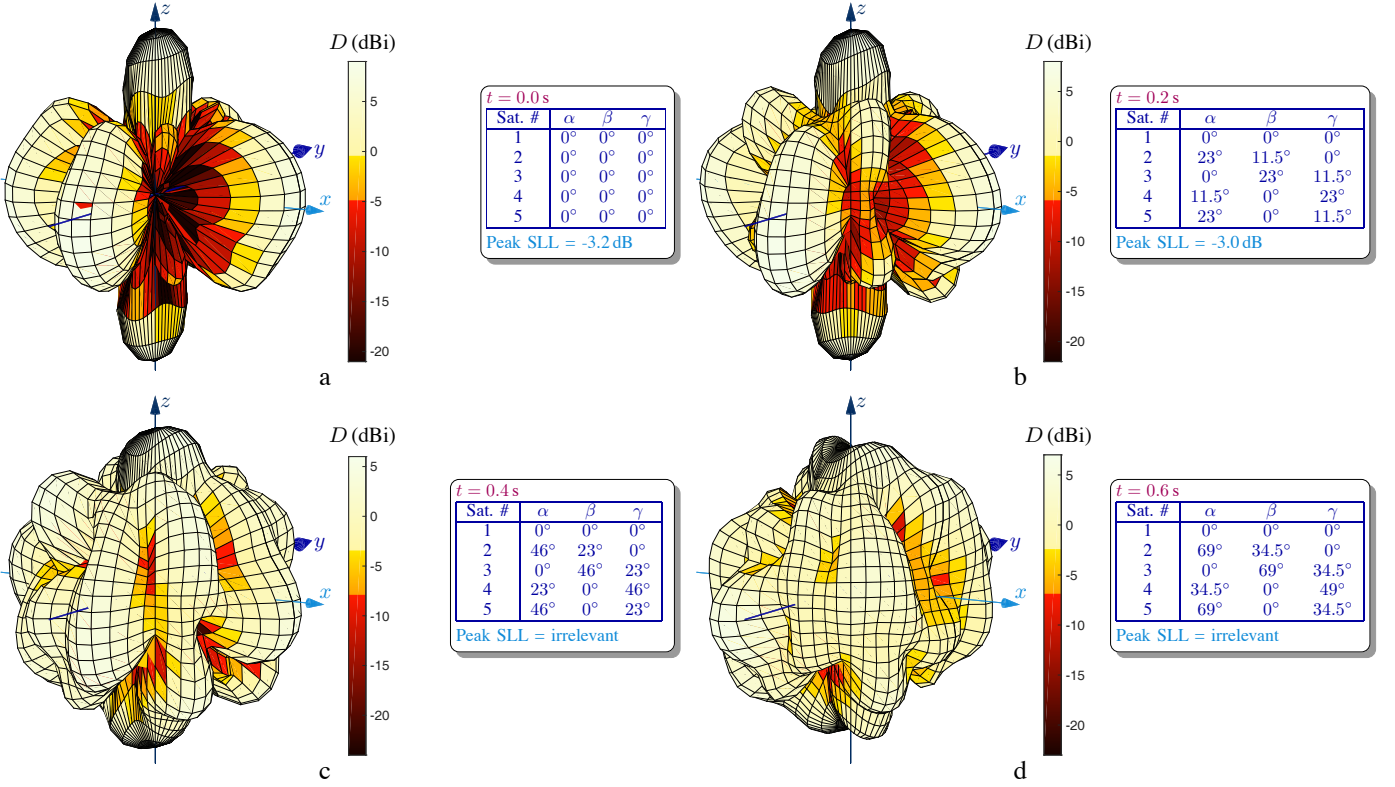
Fig. 2. Successive radiation pattern snapshots. The corresponding time instants and Euler angles are given in the tables.

$t = 0.0$ s			
Sat. #	α	β	γ
1	$0°$	$0°$	$0°$
2	$0°$	$0°$	$0°$
3	$0°$	$0°$	$0°$
4	$0°$	$0°$	$0°$
5	$0°$	$0°$	$0°$
Peak SLL = -3.2 dB			

$t = 0.2$ s			
Sat. #	α	β	γ
1	$0°$	$0°$	$0°$
2	$23°$	$11.5°$	$0°$
3	$0°$	$23°$	$11.5°$
4	$11.5°$	$0°$	$23°$
5	$23°$	$0°$	$11.5°$
Peak SLL = -3.0 dB			

$t = 0.4$ s			
Sat. #	α	β	γ
1	$0°$	$0°$	$0°$
2	$46°$	$23°$	$0°$
3	$0°$	$46°$	$23°$
4	$23°$	$0°$	$46°$
5	$46°$	$0°$	$23°$
Peak SLL = irrelevant			

$t = 0.6$ s			
Sat. #	α	β	γ
1	$0°$	$0°$	$0°$
2	$69°$	$34.5°$	$0°$
3	$0°$	$69°$	$34.5°$
4	$34.5°$	$0°$	$49°$
5	$69°$	$0°$	$34.5°$
Peak SLL = irrelevant			

implying $\hat{\xi} \to -\hat{z}$. Then, by analytic continuation, $E_\vartheta^\infty(\hat{z}) = E_\vartheta^\infty(-\hat{z}) = 0$. By observing that $\hat{\vartheta}$ can be written as

$$\hat{\vartheta} = \hat{\xi} \times \frac{\hat{\xi} \times \hat{z}}{|\hat{\xi} \times \hat{z}|}, \quad \text{for } \hat{\xi} \times \hat{z} \neq \mathbf{0} \tag{9}$$

with $|\hat{\xi} \times \hat{z}| = \sin(\vartheta)$ (no sign ambiguity arising due to $0 < \vartheta < \pi$), the applicability of (7) can be extended to the general case of a dipole oriented along a direction $\hat{d}$ as

$$\mathbf{E}_d^\infty(\hat{d}, I, l, \hat{\xi})$$
$$= \begin{cases} j\eta_0 2I \exp(-jk_0 r) \dfrac{\cos(\theta_l \hat{\xi} \cdot \hat{d}) - \cos(\theta_l)}{|\hat{\xi} \times \hat{d}|} \hat{e}_d, & \text{for } \hat{\xi} \times \hat{d} \neq \mathbf{0} \\ \mathbf{0}, & \text{for } \hat{\xi} \times \hat{d} = \mathbf{0} \end{cases} \tag{10}$$

with

$$\hat{e}_d = \hat{\xi} \times \frac{\hat{\xi} \times \hat{d}}{|\hat{\xi} \times \hat{d}|}. \tag{11}$$

Equation (10) allows expressing the far-field characteristic corresponding to a *still-standing* satellite as

$$\mathbf{E}_n^\infty(\hat{\xi}) = \sum_{k=1}^3 \mathbf{E}_d^\infty(\hat{d}_{n,k}, I_{n,k}, l_k, \hat{\xi}), \quad \text{for } n = 1, \ldots, N. \tag{12}$$

By now invoking the known 3D rotations $\alpha_n(t)$, $\beta_n(t)$ and $\gamma_n(t)$, the *time-dependent* far-field characteristic corresponding to the *rotating* satellite becomes

$$\mathbf{E}_n^\infty(\hat{\xi}, t) = \sum_{k=1}^3 \mathbf{E}_d^\infty[M_n(t)\hat{d}_{n,k}, I_{n,k}, l_k, \hat{\xi}],$$
$$\text{for } n = 1, \ldots, N. \tag{13}$$

with the matrix $M_n(t)$ being given in (14) [7, Eq. (4.46)].

Equation (13) is used in the main text.

B. Beamforming & EM radiation from sources in motion

Although performing the beamforming inside the constellation presents clear tractability advantages, its concrete realisation must account for the specificity of the EM problem at hand. Concretely, the beamforming implies the exchange of (reference) signals between the satellites in the constellation, the accuracy of the beamforming being determined by the accuracy of the *shape* and *timing* of the exchanged signals. Here, [11] has cogently demonstrated that when the transmitting and receiving units are in relative motion, the EM transfer is unequivocally relativistic in nature, this having the following pivotal consequences:

- There is no simple relationship between the transmitted and received pulses. Moreover, the interrelation between the pulse shapes is no longer a time convolution, this largely complicating the processing of the incoming signals and resulting, quite likely, in positioning and/or timing errors.

- The Lorentz contraction in space and the Lorentz time dilatation may further aggravate the relevant positioning and/or timing errors.

Simply ignoring these aspects can have egregious consequences, as demonstrated, for instance, by the NASA-ESA Cassini-Huygens mission to the Saturn moon Titan [12].

This situation is alleviated when the ratio between the sources' velocity and c_0 is such that the "low-velocity approximation" [11] applies. In such cases, [13] gives some indications

t = 0.0 s

Sat. #	α	β	γ
1	0°	0°	0°
2	0°	0°	0°
3	0°	0°	0°
4	0°	0°	0°
5	0°	0°	0°

Peak SLL = -3.2 dB

t = 0.2 s

Sat. #	α	β	γ
1	0°	0°	0°
2	23°	11.5°	0°
3	0°	23°	11.5°
4	11.5°	0°	23°
5	23°	0°	11.5°

Peak SLL = -3.3 dB

t = 0.4 s

Sat. #	α	β	γ
1	0°	0°	0°
2	46°	23°	0°
3	0°	46°	23°
4	23°	0°	46°
5	46°	0°	23°

Peak SLL = -3.1 dB

t = 0.6 s

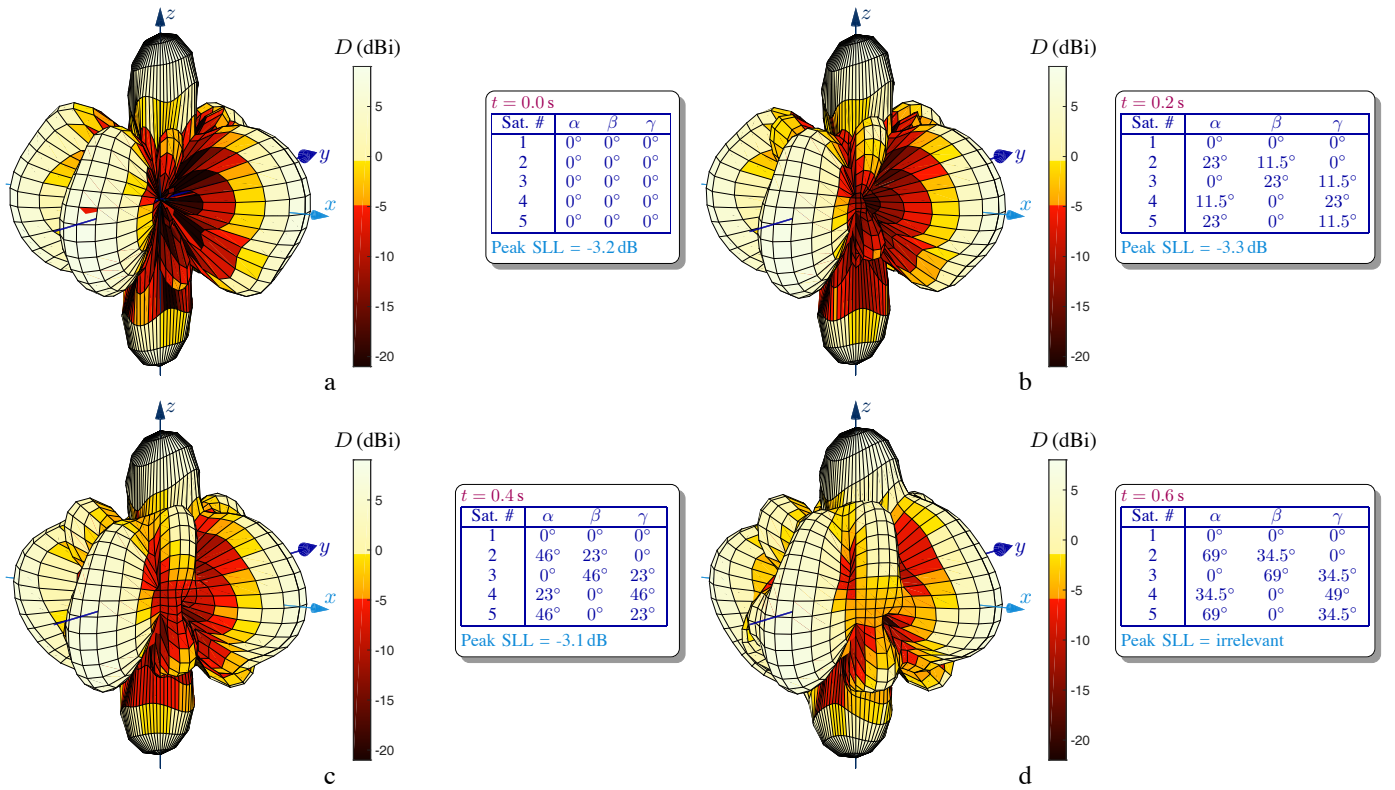| Sat. #	α	β	γ
1	0°	0°	0°
2	69°	34.5°	0°
3	0°	69°	34.5°
4	34.5°	0°	49°
5	69°	0°	34.5°

Peak SLL = irrelevant

Fig. 3. Successive integrated radiation pattern. The corresponding time instants and Euler angles are given in the tables.

$$M_n(t) = \begin{bmatrix} \cos(\beta_n)\cos(\alpha_n) & \sin(\gamma_n)\sin(\beta_n)\cos(\alpha_n) - \cos(\gamma_n)\sin(\alpha_n) & \cos(\gamma_n)\sin(\beta_n)\cos(\alpha_n) + \sin(\gamma_n)\sin(\alpha_n) \\ \cos(\beta_n)\sin(\alpha_n) & \sin(\gamma_n)\sin(\beta_n)\sin(\alpha_n) + \cos(\gamma_n)\cos(\alpha_n) & \cos(\gamma_n)\sin(\beta_n)\sin(\alpha_n) - \sin(\gamma_n)\cos(\alpha_n) \\ -\sin(\beta_n) & \sin(\gamma_n)\cos(\beta_n) & \cos(\gamma_n)\cos(\beta_n) \end{bmatrix}$$
$$\text{with } \alpha_n = \alpha_n(t), \beta_n = \beta_n(t), \gamma_n = \gamma_n(t). \quad (14)$$

on the framework to be applied for processing the interchanged signals. For this study, the approximation allows decoupling the satellites' radiation properties from their motion.

It must be noted that the intricacies pertaining to moving radiating sources would still manifest themselves when raw data were transmitted to Earth for processing. It can be expected that the larger velocities applying to that model would have a substantially more pronounced effect on the communication channel, this providing additional arguments against such a solution.

REFERENCES

[1] ESA, "SPICA - a space infrared telescope for cosmology and astrophysics," [Online]. Available: http://sci.esa.int/cosmic-vision/53635-spica/.

[2] S. Jester and H. Falcke, "Science with a lunar low-frequency array: From the dark ages of the Universe to nearby exoplanets," *New Astron.*, no. 53, pp. 1–29, Feb. 2009. [Online]. DOI:10.1016/j.newar.2009.02.001.

[3] M. J. Bentum, C. J. M. Verhoeven, A. J. Boonstra, A. J. van der Veen and E. K. A. Gill, "A Novel Astronomical Application for Formation Flying Small Satellites," in *Proc. of the 60th International Astronautical Congress*, Daejeon, Republic of Korea, Oct. 2009.

[4] R. T. Rajan, S. Engelen, M. J. Bentum, and C. J. M. Verhoeven, "The Orbiting Low Frequency Antenna Array," in *Proc. of the IEEE Aerospace*, Big Sky, Montana, USA, March. 2011.

[5] P. K. A. van Vugt, A. Budianu, A. Meijerink and M. J. Bentum, "Calibration Approach of the OLFAR Space Based Radio Telescope," in *Proc. of the 65th International Astronautical Congress*, Toronto, Canada, Sep. 2014.

[6] M. J. Bentum, I. E. Lager, S. Bosma, W. P. Bruinsma, and R. P. Hes, "Beamforming in sparse, random, 3D array antennas with fluctuating element locations," in *Proc. 9th EuCAP*, Lisbon, Portugal, Apr. 2015.

[7] H. Goldstein, C. Poole and J. Safko, *Classical Mechanics*, 3rd ed., San Francisco: Addison Wesley, 2001.

[8] I. E. Lager and M. Simeoni, "Radiation properties of non-uniform array antennas," in *Proc. 42nd EuMC*, Amsterdam, the Netherlands, Oct.-Nov. 2012, pp. 502–505.

[9] C. A. Balanis, *Antenna Theory: Analysis and Design*, 3rd ed., New York: John Wiley & Sons Inc., 2005.

[10] I. E. Lager and A. T. de Hoop, "TD radiation properties of array antennas composed of pulsed electric-current excited elements," *IEEE Antennas Wireless Propag. Lett.*, vol. 14, pp. 715–718, Mar. 2015.

[11] A. T. de Hoop, "Electromagnetic radiation from moving, pulsed source distributions: The 3D time-domain relativistic Doppler effect," *Wave Motion*, vol. 46, pp. 74–77, Aug. 2008.

[12] J. Oberg, "Titan calling," *IEEE Spectrum*, vol. 41, no. 10, pp. 28–33, Oct. 2004.

[13] A. T. de Hoop, "Fields and waves excited by impulsive point sources in motion – The general 3D time-domain Doppler effect," *Wave Motion*, vol. 43, pp. 116–122, Sep. 2005.

[14] A. Budianu, A. Meijerink, M. J. Bentum, D. M. P. Smith, and A.-J. Boonstra, "Antenna architecture of a nano-satellite for radio astronomy," in *Proc. 2014 IEEE Aerospace Conference*, Big Sky, MT, pp. 1–10, Mar. 2014.